

A cosmic ray cocoon along M87’s jet?

M.G. Dainotti^{1,3}, M. Ostrowski¹, D. Harris², A. Siemiginowska², H. Siejkowski¹

¹ *Observatorium Astronomiczne, Uniwersytet Jagielloński, ul. Orla 171, 30-244 Kraków, Poland*

² *Smithsonian Astrophysical Observatory, 60 Garden Street, Cambridge, MA 02138, USA*

Accepted xxx, Received yyy, in original form zzz

ABSTRACT

Relativistic jets propagating through an ambient medium must produce some observational effects along their side boundaries because of interactions across the large velocity gradient. One possible effect of such an interaction would be a sheared magnetic field structure at the jet boundaries, leading to a characteristic radio polarization pattern. As proposed by Ostrowski, another effect can come from the generation of a high energy cosmic ray component at the boundary, producing dynamic effects on the medium surrounding the jet and forming a cocoon dominated by cosmic rays with a decreased thermal gas emissivity. We selected this process for our first attempt to look for the effects of this type of interaction. We analyzed the Chandra X-ray data for the radio galaxy M87 in order to verify if the expected regions of diminished emissivity may be present near the spectacular X-ray jet in this source. The detailed analysis of the data, merged from 42 separate observations, shows signatures of lower emissivity surrounding the jet. In particular we detect an intensity dip along the part of the jet, which would be approximately 150 pc x 2 kpc in size, if situated along the jet which is inclined toward us. Due to a highly non-uniform X-ray background in the central region we are not able to claim the discovery of a cosmic ray cocoon around the M87 jet: we only have demonstrated that the data show morphological structures which could be accounted for if a cosmic ray cocoon exists.

Key words: galaxies: active, jets, acceleration of particles

1 INTRODUCTION

M87 (NGC 4486) is a dominant radio galaxy in the center of the Virgo cluster, at a distance of $D = 16$ Mpc (Tonry 1991) so that $1'' = 77$ pc. It hosts a 3.2×10^9 solar masses super-massive black hole (Harms et al. 1994; Ford et al. 1994; Macchetto et al. 1997) and a relativistic jet (Sparks et al. 1996; Perlman et al. 2001; Marshall et al. 2002; Harris et al. 2003). The first Chandra observations of M87 that specifically targeted the jet were those by Wilson in 2000 July (Wilson & Yang 2002; Perlman & Wilson 2005). On larger scales M87 has been the subject of detailed radio observations showing remarkable structures on scales up to 40 kpc (Owen et al. 2000; Hines & Owen 1989). In soft X-rays, M87 is the second brightest extragalactic source (after the Perseus cluster) and the emission is dominated by the thermal radiation from its ~ 2 keV gaseous atmosphere c.f., (Molendi 2002; Gorenstein et al. 1997; Fabricant & Gorenstein 1983; Boringer et al. 2001; Matsushita et al. 2002; Belsole et al. 2001).

Here we investigate the surface brightness profiles across the M87 jet in the X-ray band (0.3 – 7.0 keV), observed by Chandra to search for possible effects of a relativistic jet on the ambient medium of the host galaxy caused by high-energy cosmic rays (CRs) accelerated at the jet side bound-

ary, see Ostrowski (2000). In extreme cases, such accelerated cosmic rays are expected to be able to push the ambient medium off the jet, creating a ‘cosmic ray dominated cocoon’, separating the jet from the surrounding medium. The mechanism becomes efficient provided the velocity difference across the jet boundary is relativistic and a sufficient amount of turbulence is generated in the medium; see Ostrowski (1990; 1998; 2000).

Dynamic effects caused by CRs depend on the ratio of the CR pressure, P_{cr} , to the ambient medium pressure, P_{ext} , at the jet boundary. If, at small CR energies, the acceleration time scale is longer than the jet dynamic time or the particle escape is efficient, the resulting energetic particle population cannot reach a sufficiently high energy density to produce dynamic effects. In this case CRs act only as a viscous agent near the boundary, decreasing slightly the gas and magnetic field concentration in this region, see also in Arav & Begelman (1992). In such cases we call the cylindrically distributed cosmic ray population a ‘weak cosmic ray cocoon’. Then, if the accelerated particles are electrons or can transfer energy to electrons, a specific cosmic ray electron population is formed along the jet leading to a characteristic synchrotron component with slowly varying spectral index and break frequency. The energy density of such radiating electrons is expected to have its maximum in a cylindrical

layer at the jet boundary^{*}. However, if the energy losses are not significant at low energies and the acceleration process is fast enough, the cosmic ray pressure could reach values comparable to the medium pressure, leading to a substantial modification of the jet boundary layer. There are various possibilities arising in such cases (*‘dynamic cosmic ray cocoons’* (Ostrowski 2000)) depending on the conditions near the jet and on the effects of a CR backreaction on the efficiency of the acceleration process. The cosmic ray pressure may stabilize at an intermediate pressure $P_{\text{cr}} < P_{\text{ext}}$, or grow to form the dynamic cosmic ray cocoon, as one can see in Fig. 3 in Ostrowski (2000).

Let us consider a possible scenario of dynamic interaction of high energy cosmic rays with the jet and the ambient medium. The particles are injected and accelerated at the jet boundary. Growing numbers of such particles result in forming the cosmic ray pressure gradient outside the jet pushing the ambient medium aside. Additionally, an analogous gradient may be formed directly into the jet, helping to keep it collimated. The resulting rarefied or partially empty portion of the ambient medium cylindrical volume along the jet will decrease the acceleration efficiency. Thus the cosmic ray energy density may build up only to a value comparable to the ambient medium pressure, when it is then able to push the ambient medium away, because the diffusive escape of charged particles from the cosmic ray cocoon is not expected to be efficient (contrary to photons considered by Arav & Begelman (1992)). In some cases the evacuated volumes could be quite large, reaching values comparable to the jet’s radius, or even larger, expanding into the hot ambient gas. The accumulated cosmic rays can be removed by advection in the form of CR bubbles or CR dominated winds outside the active nucleus, moving into regions of more tenuous medium, or they can simply diffuse outside the jet at larger distances from the central source. In all of these cases, one may expect a decrease of the thermal emissivity near the jet – in the CR dominated cocoon – leaving an observational signature of the CR related process. In the present paper we attempt to verify such a model using X-ray observations of the jet in the galaxy M87, searching for a lower emissivity volume along the jet. In Section 2 we present the data analysis, in Section 3 the evidence and explanation of the soft X-ray structures in the M87 central region, in Section 4 the physical constraints for the cosmic ray cocoon and in the final remarks we discuss the existence of an X-ray morphological structure along the M87 jet, which could be an indication of a cosmic ray cocoon.

2 DATA ANALYSIS

We have selected 42 observations of M87 obtained by the Chandra AXAF CCD Imaging Spectrometer (ACIS). Amongst these are the longest observations but we have also included the majority of the 5ks ACIS-S monitoring observations with 0.4s frame time. Since we focused our analysis on a jet segment far enough removed from HST-1, we only avoided using 5ks observations during the time HST-1 was

Table 1. A list of observations and their exposure times used in the present analysis, with a separation of the chip 7 data (top) and the chip 3 data (bottom).

<i>ObsID</i>	<i>Exposure</i> [ks]	<i>Date</i>
10282	4.70	2008-11-17
10283	4.70	2009-01-07
10284	4.70	2009-02-20
10285	4.66	2009-04-01
10286	4.68	2009-05-13
10287	4.70	2009-06-22
1808	14.7	2000-07-30
3084	5.13	2002-02-12
3085	5.39	2002-01-16
3086	5.09	2002-03-30
3087	5.48	2002-06-08
3088	5.19	2002-07-24
3975	5.83	2002-11-17
3976	5.28	2002-12-29
3977	5.82	2003-02-04
3978	5.35	2003-03-09
3979	4.95	2003-04-14
3980	5.28	2003-05-18
7350	5.14	2007-02-13
7351	5.16	2007-03-24
7352	5.06	2007-05-15
7353	5.01	2007-06-25
7354	5.19	2007-07-31
8510	4.70	2007-02-15
8511	4.70	2007-02-18
8512	4.70	2007-02-21
8513	4.70	2007-02-24
8514	4.47	2007-03-12
8515	4.69	2007-03-14
8516	4.67	2007-03-19
8517	4.67	2007-03-22
8575	5.16	2007-11-25
8576	5.17	2008-01-04
8577	5.14	2008-02-16
8578	5.19	2008-04-01
8579	5.19	2008-05-15
8580	5.19	2008-06-24
8581	5.13	2008-08-07
2707	99.93	2002-07-06
7212	66.11	2005-11-14
5826	128.44	2005-03-03
5827	158.27	2005-05-05

extremely bright. The total observing time is ≈ 634 ks. In Table 1, information about the analyzed data is presented.

We started our analysis with the longest single observation obsid 5827. Our results showed a region near the jet with lower surface brightness between knots E and A, Fig. 1. Motivated by this first result we merged all the available data to increase considerably the number of counts in order to perform a detailed analysis of the emission surrounding the jet.

2.1 Merging procedure

Before starting the data merging procedure in all observations, we corrected the nominal RA and Dec in the fits

^{*} Or at relativistic velocity jump interfaces between jet components, as proposed previously (Meliani & Keppens 2009)

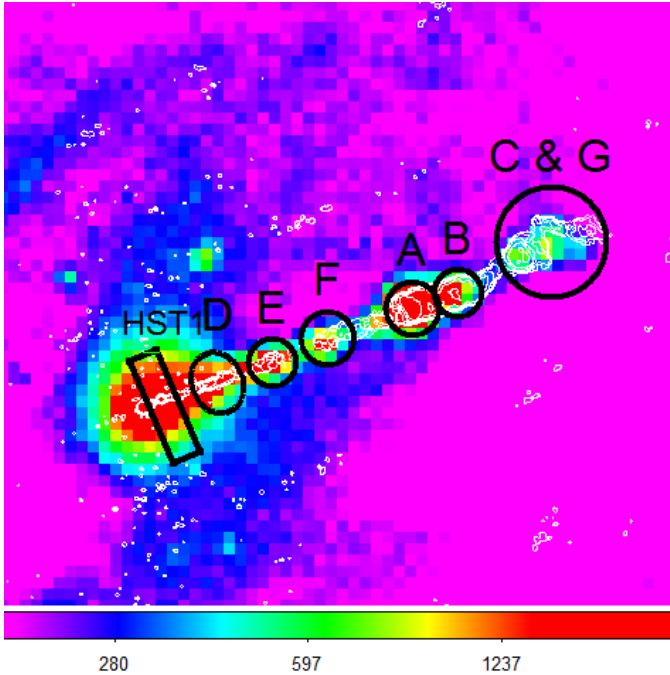


Figure 1. The merged image without any smoothing or binning. The energy band is 0.3 – 2.0 keV and VLA radio contours are superimposed. In the picture, between knots E and A, one can note a dip in X-ray intensity on the north side of the jet. A circle around knot F shows a region used for verification of the data merging procedure. Distances of the knots from the central black hole: HST-1: $0.8'' - 1.2''$, D: $2.7'' - 4''$, E: $5.7'' - 6.2''$, F: $8.1'' - 8.8''$, I: $10.5'' - 11.5''$, A: $12.2'' - 12.5''$, B: $14.1'' - 14.5''$, C: $17.5'' - 19''$. Every pixel in any image is $0.492''$ and $1'' = 77$ pc, the projected length of the jet from the core to knot C is ≈ 1.5 kpc.

header in order to ensure that the celestial location of the observed nuclear X-ray emission coincided with the radio position of the nucleus. This procedure didn't change the physical coordinates of events. Then, we applied the simple merging procedure “merge all” from CIAO (Chandra Interactive Analysis of Observations)[†] tools, version 4.2. We merged observations from different chips since we are interested in a morphological analysis and not in the spectral properties of the merged image. In particular, we are looking for the features of decreasing emissivity, called ‘dips’, along the M87 jet. We obtained a picture without any systematic offset in the World System Coordinates (WCSs) of the observations. However, to be sure that the simple merging procedure was sufficient to guarantee a correct image we checked that the counts in a circular region on knot F of the merged image was equal to the sum of the counts of the individual images at the same position. We also created exposure maps and merged exposure map of all the observations used in the analysis to check that the exposure map was uniform across the regions close to the jet.

[†] <http://asc.harvard.edu/ciao>

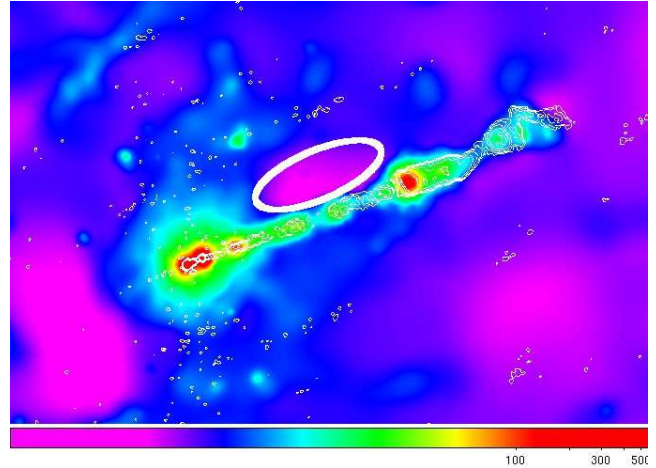


Figure 2. An adaptively smoothed image in the 0.3–2 keV energy range, with the VLA radio contours superimposed. The lower surface brightness region on the north side of the jet is indicated by an elliptical region.

2.2 Morphological analysis of the merged data

In order to perform a detailed analysis of the X-ray surface brightness near the jet we have split and analysed the merged data into a few selected energy bands: 0.3 – 0.8 keV, 0.8 – 1.2 keV, 1.2 – 2.0 keV, 2.0 – 4.0 keV, 4.0 – 7.0 keV and an additional wider soft band 0.3 – 2.0 keV, to look for an energy dependent morphology. In Fig.1 we show the merged image in the soft band 0.3 – 2keV, where the most visible dip structures appear; they are less pronounced at higher photon energies. Close to the jet, the ISM is cool and dense, producing the complex surface brightness structures we see in the central region. The harder X-rays however arise from hotter and less dense gas in the outer parts of the galaxy, and the surface brightness above 2 or 3 keV will be produced mostly by the integrated emissivity along the line of sight rather than by discrete features near the jet. Thus we do not expect to see any indication of a CR cacoon at higher energies. Between knots F and E one can note a feature of lower brightness that is visible especially on the north side of the jet. The analogous dip is present next to knot F on the south side of the jet, but it is less remarkable. The mentioned dip structures are more clearly visible for the same data, both on the north and south side when we apply the adaptive smoothing tool, *csmooth*, as illustrated in Fig. 2. We note here that the interpretation of the maps is not straightforward due to confusion with the non-uniform thermal background emission near the centre of M87.

For Fig. 2 we have used *csmooth*. The *csmooth* procedure creates a reference scale map (in this case using the 0.3–2.0 keV data) and we used this scale map for the other energy bands[‡]. In the analysis we have also tested other smoothing techniques provided in the CIAO software: the Quadtree binning with *dmnautilus* and *aconvolve* (a simple Gaussian) in order to compare the resulting pictures, but there was no visible difference or improvement in comparison

[‡] for the details on how to create maps with *csmooth* see (Balucinska et al. 2005).

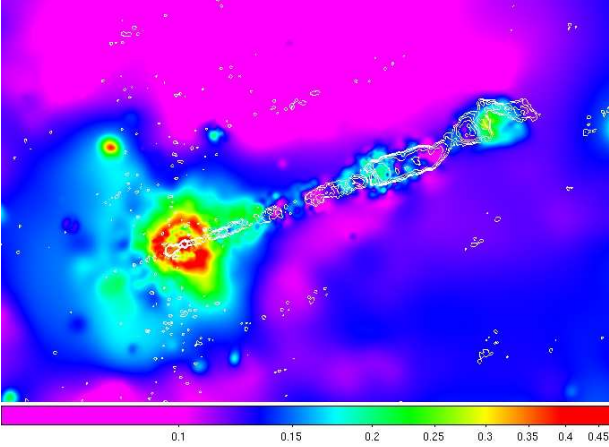


Figure 3. The hardness ratio map $HR=(2-7 \text{ keV})/(0.3-2 \text{ keV})$, overlaid with the radio contours. The structure at the galaxy centre results from the instrumental phenomenon of photon pile up.

to the data treated with *csmooth*. One should remember here that the adaptive smoothing procedure in CIAO should not be used for any quantitative analysis as it can redistribute the flux. When the kernel is variable, the *csmooth* algorithm has the effect of moving flux from low surface brightness regions into high surface brightness regions with a possibility of creating spurious emission, Diehl & Statler (2006).

2.3 Hardness ratio maps

To get additional insight into the weak emission from the dips we constructed hardness ratio maps of the jet. Let us define the hardness ratio as

$$HR \equiv \frac{H}{S},$$

where H is the hard band counts/pixel and S is the soft band counts/pixel. The HR maps are derived by dividing the *csmoothed* H and S maps using the CIAO procedure *dmimcalc*. As the reference soft energy band we have selected the 0.3 – 2.0 keV range. The smoothing pattern for this map was used to smooth the high energy band 2.0 – 7.0 and derive the HR map $H(2.0 - 7.0)/S(0.3 - 2.0)$, as presented in Fig. 3. One may see here that the jet has a harder spectrum than the surrounding gas, and there are softer regions observed between the jet knots. Also the large dip region from Fig. 1 is apparently harder than the neighbouring galactic plasma. This is consistent with the harder photons in the dip area arising from hot gas along the line of sight. No particular spectral feature which could be ascribed to the jet outer layers or to a CR cocoon is obvious.

2.4 The cross-jet intensity profiles

Using *ds9* we have analyzed perpendicular projections across the jet to visualize the intensity variations. Additionally, to be sure that the evaluation of the above mentioned features is not affected by photon pile up (when two or more photons arrive at the same pixel in the same frame time and are registered as a single event with the sum of the photon energies

(Davis 2001)), or by the spatial contamination due to flaring activity of HST-1, we have excluded from the analyzed data the observations from January 2004 up to June 2006. In this period HST-1 - the first jet knot clearly resolved by Chandra from the nuclear emission - was the site of a huge X-ray flare in 2005, Harris et al. (2009). To be even more cautious, we considered projections of the jet starting from knot E, thus avoiding effects of HST 1 variability. We tested different values of the projection width in order to optimize the signal to noise while still being able to resolve the dip. In Fig. 6, we present a profile perpendicular to the jet located at knot F of all observation and in Fig. 5 of a single observation. These clearly exhibits the lower surface brightness near the jet. A width of $2.5''$ resulted from these tests (Fig. 4). For this procedure we have binned the map to a pixel size of $0.061''$ and smoothed it with a $1.03''$ FWHM Gaussian.

As knot F looks like a point source on the map we decided to model it using the Chandra Point Spread Function (PSF) as a point source imposed on the local background. To perform the PSF fitting we used the longest single observation, obsid 5827, in order to extract the source spectrum that cannot be properly computed if we consider the merged file. In case of a merged image we don't have a single aspect solution since it is varying between different observations. We fitted the spectrum with a simple power law, with a photon index $\Gamma = 2.3$, applying the Galactic absorption modeled as neutral gas with the Solar abundances and a column density equal $1.94 \times 10^{20} \text{ cm}^{-2}$, the value determined by the Leiden/Argentine/Bonn (LAB) Survey of Galactic H I (Kalberla et al. 2005). The PSF map, scaled to knot F after subtracting the background near the knot, was obtained running ChaRT and MARX with Ciao 4.2. One should note that the background level near the knot was fitted here by the requirement of the best PSF fit to the knot. Then, we derived the PSF projection and subtracted it from the knot F projection, as presented in Fig. 7. It is clearly visible that the fitted background level near the jet is significantly lower than the mean fluctuating background. In Fig. 5 we show a profile of a single observation which confirms that the observed dip structure is not affected by the merging procedure of the full data set.

In all our various images there is an asymmetry between the ambient medium emission north and south of the jet, with a lower surface brightness to the north. The elongated dips are not visible along the full length of the jet and between knots E and F are much more pronounced on the north side of the jet. There is a wealth of structured emission below 2 keV in the central regions of M87 (e.g. Fig. 8). The surface brightness dip in the region along the north side of the jet, in the vicinity of knot F, can be a manifestation of a cosmic ray cocoon, but it could also be a simple void in projected background structures. In the next section we attempt to examine these possibilities.

3 THE SOFT X-RAY STRUCTURES IN THE CENTRAL REGION OF M87

3.1 Nature of the features with a decreased brightness

The central part of M87 is dominated by a bright circular region with an approximate radius of $50''$ or 3.85 kpc, although

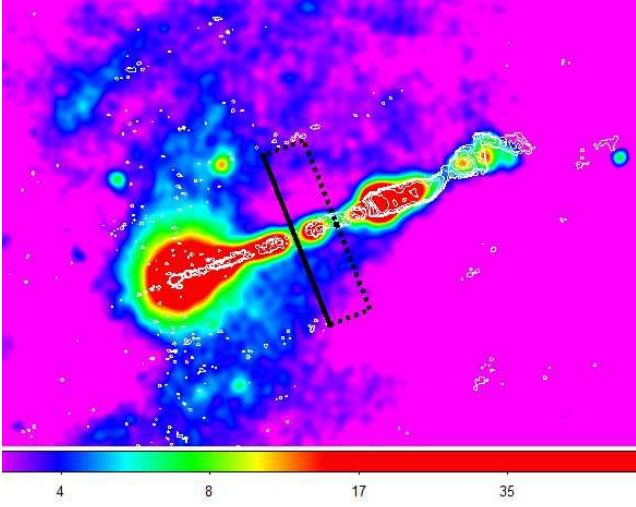


Figure 4. The region used for the projection ($2.5''$ width) across knot F in the energy band $0.3 - 2$ keV. The image is binned to a pixel size $0.061''$ and smoothed with a Gaussian of $\text{FWHM}=1.03''$.

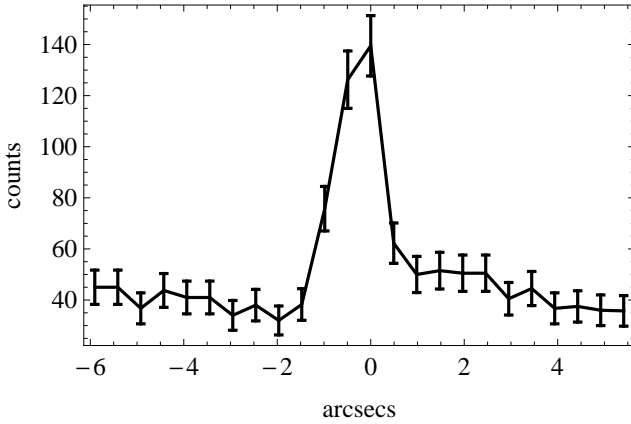


Figure 5. The projection across knot F in the energy band $0.3 - 2$ keV for the single longest observation (obsid 5827). No binning nor smoothing has been used.

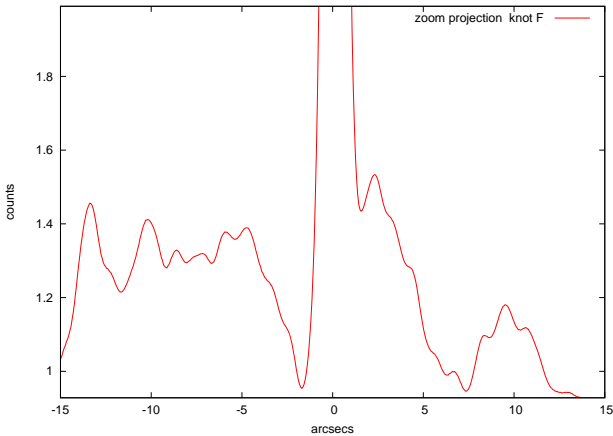


Figure 6. The projection across knot F in the energy band $0.3 - 2$ keV, binned with pixel size $0.061''$ and smoothed with a Gaussian of $\text{FWHM}=1.03''$.

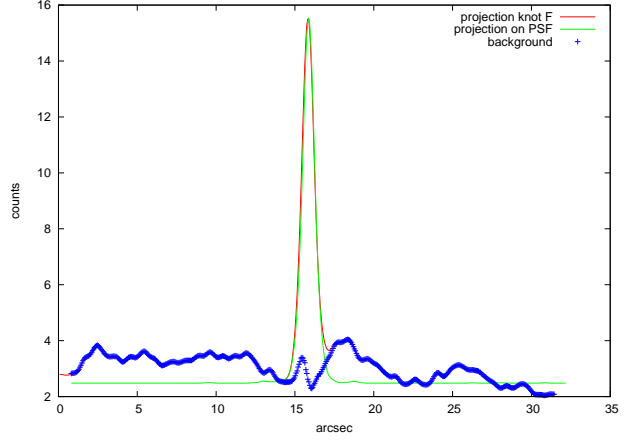


Figure 7. The background near the jet (blue curve) is obtained by subtracting the modeled PSF projection (green line) from the knot F projection (red line).

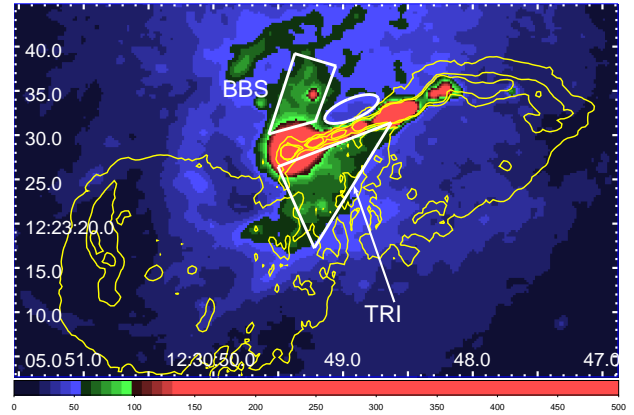


Figure 8. The M87 map with $1/4$ binning ($\text{pix}=0.123''$) and smoothing $0.43''$ FWHM. The yellow 8 GHz radio contours start at 3 mJy/beam and increase by a factor of 2 up to 48 mJy/beam . The white ellipse shows the dip position.

there are no unique sharp boundaries. Beyond this circle extend the well known ‘SW Spur’ and the ‘Eastern Arm’ – for a more extensive description see Forman et al. (2007). Within the central circular region a complex brightness distribution is observed, most clearly seen below 2 keV. At higher energies, the surface brightness contrast diminishes. In fact, if we repeat the same analysis in knot F (adopted for the low energy band and described in sec. 2.4) for the $2.0 - 7.0$ keV band, we recover a decrease in the intensity that is 6 times smaller than the one observed in the band $0.3 - 2.0$ keV. With the exception of the rims around ‘bubbles’ (Forman et al. 2007), it is difficult to isolate coherent structures on the map, although some obvious large arcs/filaments can be noted. Sparks et al. (2004) have demonstrated a spatial association between some, but not all, of the X-ray bright features with regions containing $\text{H}\alpha$ emission. They also suggest that the brighter X-ray features come from 0.8 keV gas, a bit cooler than the 1.4 keV temperature describing most of the ISM. They suggest that this cooler gas is associated with the 10^4 K gas producing the observed $\text{H}\alpha$ emission.

It is our impression that while there is undoubtedly

more than one structure along some lines of sight, most of the bright regions are likely to be higher density volumes with a depth roughly equivalent to their lateral extent. [If the entire complex of excess brightness were to be jet associated, one could imagine a “fat sausage” centered on the jet, with various higher density regions within it. We would thus be seeing an almost end-on view of the sausage and we would then expect that most lines of sight would pass through several regions of higher emissivity (Forman et al. 2007)]. Of primary interest to us are two broad swaths: a roughly triangular region (TRI) south of the jet and a ‘broad brush stroke’ (BBS) running north of the nuclear region, losing its identity after about $10''$ (Fig. 8). The triangular region extends from the south side of the jet, mostly southerly. Its top side along the jet runs from the region around the nucleus out to knot A. We find it curious that the southern triangle stops abruptly at the jet, and does not continue north; if it had gone further north, there would be no dip. It tapers as it crosses a broad horizontal region well below the jet. When radio contours are superposed (Fig. 8) it appears that the two lower sides of the triangle coincide with the edges of both lobes. While there are no sharp boundaries in the radio brightness, it is not difficult to pick a contour level that matches the X-ray excess. In reality, even if there were sharp boundaries of exclusion, they would most likely be blurred by projection effects: it is highly likely that there is significant (hidden) radio structures in the 3rd dimension since it is so difficult to identify continuity between the inner and outer radio structures.

The northern feature (‘BBS’) defines the eastern end of the dip and the jet itself acts as the long southern edge of the dip. On the north side of the jet there are no bright radio features, only low brightness and diffuse emission. Thus there are no discrete radio regions which might exclude the hot ISM and explain the existence of the dip as a normal ‘radio cavity’.

3.2 Is the dip associated with the jet?

The low brightness ‘dip’ is identified by the ellipse in Fig. 8. At 77 pc per arcsec, the elliptical region in the figure would have a projected size of approximately 400×150 pc. Since we are currently assuming the region is related to the jet, its long axis would be deprojected in the same way as the jet, taken to be at 15 ± 5 degrees to the line of sight. Thus the deprojected estimate of the size of the region would be 1.5×0.15 kpc.

The brightness level in this dip is comparable to the region beyond the end of the jet and to the area to the south of the outer end of the jet (i.e. beyond knot B). In general, the hardness ratio maps demonstrate that the spectrum of the dip is similar to the regions mentioned for the brightness comparisons. Thus it seems unlikely that the lower brightness areas could arise from absorption by excess column density along the line of sight which would be absorbing most of the emission below 1.5 keV; we would have seen much more extreme values in the HR maps if that had been the case.

In case the dip is not associated with the jet, we have a relatively isolated region of 200 to 400 pc in size, with essentially no excess emission from the denser gas responsible for the higher brightness areas which dominate the 1 keV maps.

4 PHYSICAL CONSTRAINTS FOR THE JET AND CR COCOON

Let us consider a physical situation with energetic particle acceleration occurring within the outer layers of the jet. This process produces CR particles diffusing into the ambient medium outside the jet, which push back the ISM to form a rarefied CR cocoon. Below we discuss some constraints for such a process resulting from the overall energy budget and efficiencies of particle acceleration, diffusive escape and radiative losses.

4.1 Energy budget

Let us compute the energy of the ultrarelativistic particles inside the region, together with the amount of work required for pushing the ambient gas (with the adiabatic index $\gamma_{amb} = 5/3$) back to form the CR cocoon. Assuming that the pressure of this region is equal to the pressure of the ambient gas, $P = 1.3 \times 10^{-9}$ dyn cm $^{-2}$ (Stawarz et al. 2005; Stawarz et al. 2006) at the distance of approximately 650 pc from the galaxy center and the dip volume is $V = 0.15 \times 0.15 \times 1.5$ kpc 3 , we obtain

$$E = \gamma_{cr} P \times V \approx 2 \times 10^{54} \text{ ergs} \quad (1)$$

where $\gamma_{cr} = 4/3$ is the adiabatic index for a relativistic plasma. E could be somewhat larger than the above estimate if the cocoon is more extensive but not wholly visible because of excess X-ray emission along the line of sight. A dynamical time scale for the formation of the dip is obtained as the ratio between the energy E and the jet’s kinetic power, $L_j = \eta \times 10^{44}$ erg/s (η is a dimensionless parameter and it grows with the increasing amount of cold protons in the jet ($\eta > 1$):

$$t_{dyn} = E/L_j \approx 1.7 \times 10^{10} \eta^{-1} \text{ [s]}. \quad (2)$$

Let us indicate with ζ the fraction of L_j used for the cocoon generation, i.e. the transfer of jet kinetic energy to acceleration of cosmic rays and to transport outside the cocoon. To estimate the maximum efficiency, ζ_{max} , of this process one can compare t_{dyn} with the life time of the jet, t_j . t_j must be greater than the light travel time along the jet (the distance from the nucleus to knot C, $t_{lt} \approx 2$ kpc). We thus obtain $\zeta_{max} \approx 10^{-1} \eta^{-1}$. This value seems to require quite a large CR acceleration efficiency for explaining the energetics of the cocoon. Of course, if the observed jet is a stationary structure lasting a significant number of t_{lt} , $t_j = \rho \times t_{lt}$, the required efficiency diminishes to $\zeta = \zeta_{max}/\rho$. With the jet activity time $\sim 10^6$ yrs evaluated by Bicknell & Begelman (1996) the required acceleration efficiency decreases to $\zeta_{min} \sim 10^{-4}$, a value which is quite acceptable from the energy budget point of view.

In order to consider the CR cocoon energy budget in a stationary condition one can compare the above time scale with the one describing the diffusive particle escape time scale from the cocoon volume:

$$t_{esc} \sim \frac{V^{2/3}}{\kappa_{eff}} \quad (3)$$

where $V^{2/3}$ is the squared (linear) size of the volume. To obtain a rough numerical evaluation we assume in Eq. 3 the minimum diffusion coefficient along the magnetic field (the

Bohm diffusion, see e.g. Drury 1983) for the effective diffusion coefficient, $\kappa_{eff} \approx \kappa_B \sim r_g(\epsilon)c$. With $r_g = \epsilon/eB$, one obtains a numerical value $\kappa_B \approx 10^{23} \epsilon_{GeV} B_{\mu G}^{-1} [\text{cm}^2 \text{s}^{-1}]$. Henceforth we will use a dimensionless energy $\epsilon_{GeV} \equiv \epsilon/(1\text{GeV})$ and magnetic field $B_{\mu G}$ measured in μG . Then, for a power law cosmic ray spectrum $n(\epsilon) \propto \epsilon^{-\alpha}$ within the range $\epsilon_{min} < \epsilon < \epsilon_{max}$,

$$t_{esc} \sim 10^{19} \epsilon_{GeV,i}^{-1} B_{\mu G} [\text{s}], \quad (4)$$

where $\epsilon_i \approx \epsilon_{max}$ or ϵ_{min} for flat ($\alpha < 2$) or steep ($\alpha > 2$) particle spectra, respectively. One can conclude that for the steep CR spectra with $\epsilon_{GeV,i} \leq 1$ generated at the jet side boundary $t_{esc} \geq 10^{19} \text{ s} \gg t_j \sim 10^{11} \text{ s}$ and the *diffusive escape* process can be neglected if we do not assume unrealistic conditions in the medium. On the other hand, for flat particle spectra a substantial difference may appear depending on the CR main component - electrons or protons. Let us note, following Stawarz et al. (2005), that the characteristic values of B within the jet can not be much weaker than the equipartition value of a few $\times 10^{-4} \text{ G}$. We also note that the ambient stellar light energy density ($\sim 10^{-10} \text{ erg/cm}^3$) is comparable to the magnetic field energy density. Thus we take $B_{eff} = 100 \mu\text{G}$ for our numerical evaluations within the jet volume.

4.2 CR electron content

Following Ostrowski (2000) one can evaluate the electron acceleration time scale within the boundary layer for highly relativistic electrons using a well known formula for the acceleration in the Alfvénic turbulence, $t_{acc} = \epsilon^2(v/c)^2/9\kappa_{eff}$. With $v_3 \equiv v/(3000\text{km/s})$ being a characteristic MHD turbulence velocity, the acceleration time scale

$$t_{acc,e} \sim 3 \times 10^6 \epsilon_{GeV} B_{\mu G}^{-1} v_3^{-2} [\text{s}] \quad (5)$$

while the radiative loss time scale due to synchrotron and inverse Compton processes can be written as

$$t_{rad,e} \sim 4 \times 10^{17} \epsilon_{GeV}^{-1} B_{eff,\mu}^{-2} [\text{s}] \quad (6)$$

where the “effective” magnetic field $B_{eff}^2 \equiv B^2 + 8\pi U_{amb}$ and U_{amb} is the ambient radiation energy density measured in the jet rest frame (we assume a Thompson limit for the IC scattering). Comparing the above two expressions, with $v_3 = 1$ and $B_{\mu G} = 100$ within the jet volume, yields the maximum electron energy as $\epsilon_{max} \sim 3.7 \times 10^4 \text{ GeV}$. Thus the escape time $t_{esc} \sim 10^{15} B_{\mu G} \text{ s}$ is much longer than all other time scales both for the jet volume and for the (weak $B \sim 1 \mu\text{G}$) cocoon. Therefore, independent of the detailed shape of the particle spectrum, diffusive particle escape can not influence the cocoon structure if the jet is purely leptonic. Also, it may be difficult to diffusively transport the accelerated electrons from the jet into the cocoon, suggesting the likelihood of an energetic proton content for the cocoon.

One may note that for the medium transported within the jet, the available acceleration time scale must be smaller than $t_{lt} \approx 2 \times 10^{11} [\text{s}]$, the turbulent medium transport time in the jet. With Eq. 5 this requirement imposes an upper limit for the accelerated particle energy $\epsilon_{lt} \approx 0.7 \times 10^5 B_{\mu G} v_3^2 \text{ GeV}$.

4.3 CR proton content

In eq. 5, by neglecting the acceleration of the jet velocity gradient (cf. Ostrowski 2000), we find an upper limit for the proton acceleration time scale. The radiative loss time scale for protons (Rachen & Biermann 1993):

$$t_{rad,p} = 5 \times 10^{24} B_{\mu G}^{-2} (1 + aX)^{-1} \epsilon_{GeV}^{-1} [\text{s}], \quad (7)$$

where a is the ratio of the energy density of the ambient photon field relative to that of the magnetic field and X is a quantity for the relative strength of (p, γ) interactions compared to synchrotron radiation. Comparing the acceleration and radiative losses time scales, with $aX = 100$, yields the maximum energy of accelerated protons $\epsilon_{GeV,max} \approx 1.3 \times 10^7$ ($\sim \epsilon_{lt}$). For such energies, or larger in the case of a contribution to the acceleration process from the neglected velocity gradient processes or $v_3 > 1$, the diffusive time scale $t_{esc,p} \sim 10^{12} \text{ s}$ becomes comparable or smaller than $t_{lt} \sim 10^{11} \text{ s}$ and one may expect a significant outflow of cosmic ray protons from the jet into the forming cocoon (note that evaluation of t_{esc} considered the Bohm diffusion limit leading to the maximum possible time scale).

A non-negligible density of cold protons, n_g , within the jet can limit the maximum CR proton energy due to (p,p) interactions. With an approximately constant p-p scattering cross section, $\sigma_{pp} \approx 3.4 \times 10^{-26} \text{ cm}^2$, the respective scattering time scale

$$t_{pp} \approx 10^{15} n_g^{-1} [\text{s}], \quad (8)$$

is much longer – for “reasonable” densities $n_g \simeq 1 \text{ cm}^{-3}$ – than the jet travel time t_{lt} . Thus, one does not expect to observe any gamma ray signature of the energetic protons within the jet, but such emission could be present from the extended interstellar medium within the M87 galaxy, with a total flux below $0.1 \zeta_{min} L_j \sim 10^{39} \text{ erg/s}$, and below the presently observed gamma ray fluxes from this source.

5 FINAL REMARKS

In this study we describe an X-ray structure along the M87 jet which could be an indication of a cosmic ray cocoon. However, any definite claim is not possible for this source because of the highly non-uniform X-ray brightness arising from high density structures in the ISM near the centre of the galaxy. The data show a clear emission dip along the north side of the jet near knots E and F, and some weak indications of decreased emissivity in other parts of the jet. We do not observe any spectral peculiarity or radio structure related to the mentioned dip, which would suggest - assuming it is a part of a CR cocoon - that the pressure inside this structure is provided by the CR nucleonic component.

Following estimates of Stawarz (2006) we have computed the energy of the ultrarelativistic particles inside that region, assuming that the pressure of this component is equal to the pressure of the ambient gas. Order of magnitude analysis of the cosmic ray acceleration and transport processes suggest that the formation of a cocoon requires the generation of a very energetic proton component, with a flat energy spectrum extending up to $\sim 10^{16} \text{ eV}$. If the existence of a CR cocoon were to be confirmed, it would imply the acceleration of protons up to extremely high energies in FRI jets.

A more conventional explanation of the dip might be a large blob of very hot, rarefied gas which would not contribute significantly to the soft X-ray emission in this region. It is not clear how to produce such a large (at least 150 x 400 pc) hot cavity without a significant amount of molecular gas in the galaxy and without a high star formation and supernovae rate. Another possibility for explaining the dip would be if a majority of the X-ray emitting gas is in the form of clouds or filaments within a the hotter gas. Then the dip could be a region along a given line of sight free of the denser medium simply by chance. It would additionally require that the observed dip elongation along the jet would appear by chance.

However, if we use an explanation such as Scenario 2 for the structures along the jet we are left with the open question about the processes acting at the jet side boundary and the interface separating it from the ambient medium. With the large tangential velocity jump across this layer one can not expect that nothing dynamic will happen there. We may note that there are other objects with regions of decreased brightness along the jet, like the radio source 3C270 and its wedge-like depressions in diffuse X-ray surface brightness surrounding the jets, Worral (2010). Therefore, we are considering a wider programme of multiwavelength studies in order to answer questions about physical structures of the jet side boundaries and of physical processes acting there.

6 ACKNOWLEDGMENT

We thank Edoardo Trussoni for valuable comments, W. Forman and W. Sparks for discussions on the vagaries of the hot ISM, M. Paolillo, A. Gibiec and A. Szostek for comments and discussions on data analysis techniques, and L. Stawarz for valuable criticism and advice. MGD and MO are grateful for the support from Polish MNiSW through the grant N N203 380336. MGD is also grateful for the support from Angelo Della Riccia Foundation. This research is funded in part by NASA contract NAS8-39073 and NASA grant GOO-11120X.

REFERENCES

Arav, N., Begelman M.C., 1992, ApJ, 401, 125
 Balucinska-Church, M., Ostrowski, M., Stawarz, L., Church, M. J., 2005, MNRAS, 357L, 6B
 Bicknell, B.V., Begelman, M.C., 1996, ApJ, 467, 597
 Belsole, E. et al., 2001, A&A, 365, L188B
 Bohringer, H., et al., 2001, A&A, 365, L181
 Davis, J. E. 2001, ApJ, 652, 575
 Diehl S., & Statler, T., 2006, MNRAS. 368, 497D
 Di Matteo T., Allen S. W., Fabian A. C., Wilson A. S., Young A. J., 2003, ApJ, 582, 133
 Drury, L.O'C., 1983, Rep. Prog. Phys., 46, 973
 Fabricant D., & Gorenstein, 1983, ApJ, 267, 535
 Ford, H. et al., 1994, ApJL, 435, L27
 Forman, W. et al., 2007, ApJ, 665, 1057.
 Gorenstein, P., Fabricant, D., Topka, K., Tucker, W., Harnden, F., 1977, ApJ, 216, L95
 Hines, D., Eilek, J. & Owen, F. 1989, ApJ, 347, 713
 Harms, R. J., et al. 1994, ApJ, 435, L35
 Harris, D., Biretta, J., Junor, W. , Perlman, E., Sparks, W. & Wilson, A., 2003, ApJL, 586, L41

Harris, D., C. C. Cheung, L. Stawarz, J. A. Biretta & E. S. Perlman 2009, ApJ, 699, 305 H
 Kalberla, P. M. W., Burton, W. B., Hartmann, D., Arnal, E. M., Bajaja, E., Morras, R., Poppel, W. G. L., 2005, A & A 440, 775
 Macchetto, F., Marconi, A., Axon, D. J., Capetti, A., Sparks, W., & Crane, P., 1997, ApJ, 489, 579
 Marshall H. L., Miller B., Davis D., Perlman E., Wise M., Canizares C., Harris D., 2002, ApJ, 564, 683
 Meliani, Z. & Keppens, R., 2009, ApJ, 705, 1594M
 Matsushita, K., Belsole, E., Finoguenov, A. & Bohringer, H., 2002, A&A, 386, 77
 Molendi, S., 2002, ApJ, 580, 815
 Owen, F., Eilek, J. & Kassim, N. 2000, ApJ, 543, 611
 Ostrowski, M., 2000, MNRAS, 312, 579
 Ostrowski, M., 1998, A&A, 335, 134O
 Ostrowski M., 1990, A&A, 238, 435
 Perlman, E. S., Biretta, J. A., Sparks, W. B., Macchetto, F. D., & Leahy, J. P., 2001, ApJ, 551, 206
 Perlman, E. S., & Wilson, A. S. 2005, ApJ, 627, 140
 Rachen, J. P., & Biermann, P., 1993, A&A, 272, 161
 Sparks, W. B., Biretta, J. A., & Macchetto, F., 1996, ApJ, 473, 254
 Sparks, W. B., Donahue, M., Jordn, A., Ferrarese, L., Ct, P., 2004, ApJ, 607, 294S.
 Stawarz L., Siemiginowska A., Ostrowski M., Sikora M., 2005, ApJ, 626, 120
 Stawarz, L. F. Aharonian, J. Kataoka, M. Ostrowski, A. Siemiginowska & M. Sikora, MNRAS, 2006, 370, 981.
 Tonry, J. L., 1991, ApJ, 382, L109.
 Wilson, A. S. & Yang Y., 2002, ApJ, 568, 133W
 Worral, D. M. et al., 2010, MNRAS, 408, 701